High harmonic generation governed by edge states in triangular graphene quantum dots

Suresh Gnawali ⬤ and Vadym Apalkov

Department of Physics and Astronomy, Georgia State University, Atlanta, Georgia 30303, USA

We study theoretically interaction of short optical pulses with triangular graphene quantum dots. If such quantum dots have zigzag edges then there are in-gap degenerate edge states, the number of which depends on the size of the system. We show that the nonlinear optical response, such as high harmonic generation, of triangular quantum dots is sensitive to the initial electron population of their edge states. In general, the emission spectra of quantum dots have weak dependence on the number of occupied edge states, but if half of the edge states are initially occupied, which can be realized only in the quantum dots with even number of edge states, then the even high harmonics are strongly suppressed. The suppression is the strongest when the frequency of the pulse is well below the band gap and it is weak when the pulse frequency becomes comparable to the band gap of the system.

I. INTRODUCTION

Interaction of optical pulses with solids and gases is characterized by nonlinear effects, such as nonlinear absorption and high harmonic generation (HHG) [1–9]. The generation of high harmonics, which is due to highly nonlinear electron dynamics in the field of the pulse, results in efficient frequency conversion, for example, conversion of visible light into extreme ultraviolet light. The HHG has been observed experimentally both in gases, i.e., in systems with randomly positioned atoms, and in solids, where the atoms have periodic spatial arrangements. The physics behind the generation of high harmonics in these two systems is different. HHG in gases occurs through a three-step process, which is a tunnel ionization of an electron, its acceleration in a laser field, and a subsequent recollision with the same atom [1,10]. In solids, the distance between the atoms is small enough and the recollision after electron excitation can occur with a different atom. Also, in solids, the generation of high harmonics is usually described in terms of interband and intraband electron dynamics [4–6,11–13]. Within this picture, the field of a pulse redistributes electrons between the bands of a solid, which is described by the interband dynamics, and the excited electrons are transferred through the nonparabolic bands, which results in nonlinear intraband electron dynamics. The high harmonics are generated during both of these processes and depending on the band gap of a solid and the frequency of a pulse, either interband or intraband dynamics gives the main contribution to HHG. One of the differences in HHG in solids and gases is the dependence of the HHG energy cutoff on the amplitude of the pulse. While, for solids, such dependence is linear [4], for gases, the HHG energy cutoff has linear dependence on the pulse intensity [1].

To observe the high harmonics in solids, which are generated by a short optical pulse, the intensity of the pulse should be relatively large, with the corresponding amplitude that is comparable to internal electric fields in solids. Such strong and short pulses were intensively used to control the

transport and optical properties of solids [14–27]. Such control is determined by ultrafast nonlinear electron dynamics in the field of the pulse. The nonlinear electron dynamics and correspondingly the generation of high harmonics can be tuned by changing the band gap of the material, the level of the internal disorder, and also by changing the dimensionality of solids going from 3D to 2D, then to 1D, and finally to zero-dimensional systems. Zero-dimensional systems or quantum dots (QDs) [28,29] have a finite size and a finite number of atoms of the corresponding solid. They can be also considered as very large artificial atoms with quasiperiodic spatial structure. Due to dimensional quantization, the energy spectra of QDs are discrete, which results in unique optical properties of QDs and the possibility to use them as an energy storage [30–34]. Although the energy spectra of QDs are discrete, generally, the corresponding QDs' states can be identify as belonging to the conduction of valence bands of the original solid. The electron dynamics in a QD in the field of an optical pulse can be described as transitions between QD states. Thus, such a dynamics can be also described as a combination of intraband and interband dynamics. Generation of high harmonics in quantum dots is a manifestation of nonlinear features of both intraband and interband dynamics. For small QDs, electron transitions to continua that are similar to the ones in gases become important. Thus, by varying the size of a QD, it is possible to trace a transformation of a HHG spectrum from the atomic one to the crystalline solid one [35]. In Ref. [35], it was shown that such a transformation occurs for a QD that consists of just six atoms.

In addition to discrete energy spectra of QDs, QDs of topological materials can have some other interesting features. Namely, under some conditions, there are in-gap edge states, which can change the nonlinear optical response of such QDs. One of the topological materials with nontrivial in-gap edge states is graphene [36–39]. Graphene is a monolayer of carbon atoms with honeycomb crystal structure [40,41], which results in a specific relativistic low-energy dispersion of the Dirac type [42–45]. A graphene monolayer placed in a strong

optical pulse shows interference patterns in the conduction band population distribution in the reciprocal space [46]. When the inversion symmetry of graphene is broken, e.g., in graphene-like materials such as transition-metal dichalcogenides, an ultrashort circularly polarized optical pulse produces a finite residual valley polarization [24,47]. In graphene QDs, the nonlinear optical response, which depends on the size and the shape of QDs, is also expected. For example, the nonlinear absorption by graphene QDs of different sizes has been reported theoretically in Ref. [48], while the HHG from a small hexagonal graphene QD with just 24 atoms has been studied numerically in Ref. [49], where the dependence of the HHG spectra on the relaxation rate has been reported. In graphene QDs considered in Ref. [48] there are no edge states due to the hexagonal shape of the QDs. At the same time, if a graphene QD has zigzag edges, then there are corresponding in-gap degenerate edge states. Such edge states can be populated by electrons, for example, by applying a gate potential. The population of the edge states follows the atomic physics Hund's rule, which is also valid for graphene QDs; see Ref. [50]. The dependence of HHG in CdSe and CdS quantum dots has been studied experimentally in Ref. [51] for quantum dots of small sizes, 2 and 3 nm.

In the present paper, we consider nonlinear optical properties of graphene QDs with zigzag edges, which can be partially occupied. We characterize the nonlinear optical response of such graphene QDs in terms of HHG. The population of the in-gap edge states before the optical pulse increases the in-gap electron density, which can change the nonlinear electron dynamics in the field of the pulse and correspondingly affect the generation of high harmonics.

The paper is organized as follows. In Sec. II, we introduce the model and main equations. In Sec. III, we discuss the results, which are summarized in the concluding Sec. IV.

II. MODEL AND MAIN EQUATIONS

We consider triangular graphene QDs (TGQDs) with zigzag edges. Such QDs have in-gap edge states, which are degenerate, and the number of such states depends on the size of the TGQD. For example, for a 24-atom TGQD there are two edge states, while for a 46-atom TGQD there are four edge states. Such TGQDs are shown in Fig. 1. The system of TGQDs placed in the external field of an ultrafast optical pulse is described by the following time-dependent Hamiltonian:

$$H(t) = H_0 + H'(t). \quad (1)$$

Here, H_0 is the field-free Hamiltonian that describes the TGQD electron system within the tight-binding model. The corresponding tight-binding Hamiltonian has the following form:

$$H_0 = -t \sum_{\langle ij \rangle} (\hat{c}_i^\dagger \hat{c}_j + \text{H.c.}), \quad (2)$$

where i and j label the sites of the TGQD, $\hat{c}_i^\dagger$ and $\hat{c}_i$ are creation and annihilation operators for an electron at site i, and $t = -2.8$ eV is the hopping integral. For a TGQD consisting of N atoms, numerical diagonalization of the tight-binding Hamiltonian (2) gives N electron levels with wave functions ψ_n and the corresponding energies E_n.
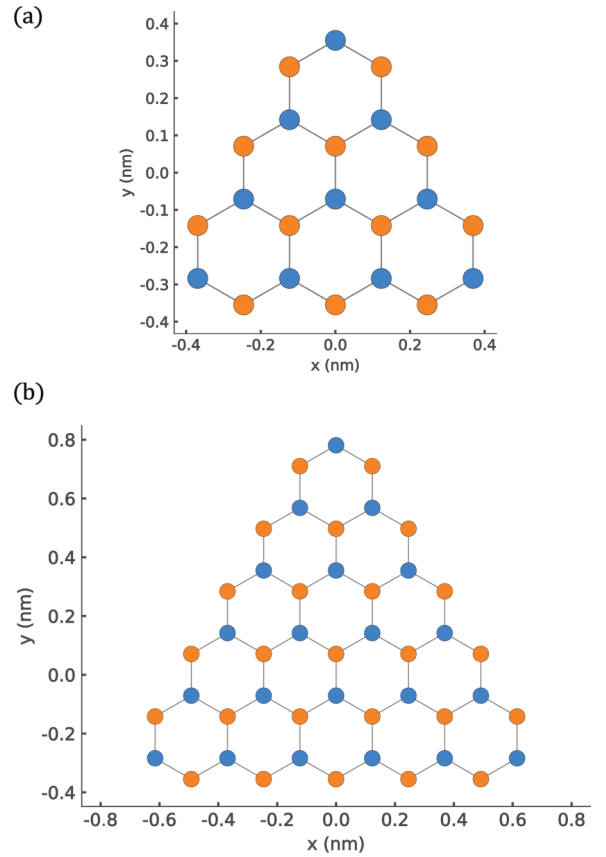

FIG. 1. Triangular graphene quantum dots with zigzag edges. The quantum dots consist of 22 atoms (a) and 46 atoms (b). The distance between the nearest-neighbor atoms is $a = 1.42$ Å.

Interaction of the TGQD with an optical pulse is described within the length gauge with the following interaction Hamiltonian,

$$H'(t) = -e \sum_i \hat{c}_i^\dagger \hat{c}_i \mathbf{r}_i \cdot \mathbf{F}(t), \quad (3)$$

where $\mathbf{r}_i$ is the position of the ith atom and $\mathbf{F}(t)$ is the time-dependent electric field of an optical pulse. Below we only consider a linearly polarized optical pulse with the profile of the following form,

$$F(t) = F_0 e^{-(t/\tau_0)^2} \cos(\omega_0 t), \quad (4)$$

where F_0 is the amplitude of the pulse, ω_0 is its frequency, and τ_0 is the duration of the pulse.

To incorporate the relaxation time, we describe the electron dynamics within the density matrix approach. With the density matrix operator $\hat{\rho}$, the dynamics of TGQDs is described by the density matrix equation

$$\frac{d\hat{\rho}}{dt} = \frac{i}{\hbar}[\hat{\rho}, H] = \frac{i}{\hbar}[\hat{\rho}, H_0] + \frac{i}{\hbar}[\hat{\rho}, H'], \quad (5)$$

where $[\hat{A}, \hat{B}]$ is the commutator of operators $\hat{A}$ and $\hat{B}$.

Taking the matrix elements of the left- and right-hand sides of Eq. (5) between the states ψ_n of field-free Hamiltonian H_0,

we obtain the following matrix equation,

$$\dot{\rho}_{mn} = i\omega_{mn}\rho_{mn} + \frac{i}{\hbar}\sum_k (\rho_{mk}H'_{kn} - H'_{mk}\rho_{kn}), \qquad (6)$$

where $\omega_{mn} = \frac{E_n - E_m}{\hbar}$, E_n is the energy corresponding to the state ψ_n, $\rho_{mn} = \langle\psi_m|\hat{\rho}|\psi_n\rangle$, $H'_{kn} = -\mathbf{D}_{kn}\mathbf{F}(t)$, and $\mathbf{D}_{kn} = e\langle\psi_k|\hat{\mathbf{r}}|\psi_n\rangle$ is the dipole matrix element of the dipole operator $e\hat{\mathbf{r}}$. The density matrix equations (6) describe the coherent electron dynamics and are equivalent to the time-dependent Schrödinger equation. The advantage of the density matrix approach is that we can include the relaxation processes into the model by introducing the corresponding phenomenological relaxation rates. The fastest relaxation processes correspond to dephasing, which are described by the relaxation of the nondiagonal matrix elements of the density matrix. We introduce the corresponding dephasing time τ, which we assume is the same for all nondiagonal matrix elements. In all calculations presented below, we assume that the dephasing time is $\tau = 10$ fs. Then the density matrix equations (6) take the following form,

$$\dot{\rho}_{mn} = i\omega_{mn}\rho_{mn} + \frac{i}{\hbar}\sum_k (\rho_{mk}H'_{kn} - H'_{mk}\rho_{kn})$$
$$- (1 - \delta_{nm})\rho_{mn}/\tau, \qquad (7)$$

where δ_{nm} is the Kronecker delta symbol.

It is convenient to introduce the interaction representation for the density matrix,

$$\tilde{\rho}_{mn} = \rho_{mn}e^{-i\omega_{mn}t}. \qquad (8)$$

Then, Eq. (7) takes the following form,

$$\dot{\tilde{\rho}}_{mn} = \frac{i}{\hbar}\sum_k [\tilde{\rho}_{mk}e^{i\omega_{nk}t}H'_{kn} - H'_{mk}\tilde{\rho}_{kn}e^{i\omega_{km}t}]$$
$$- (1 - \delta_{nm})\tilde{\rho}_{mn}/\tau. \qquad (9)$$

The system of equations (9) is solved numerically using the ODEINT library. The initial conditions, i.e., the initial populations of the TGQD levels, are defined as follows. As we discuss below, the energy spectra of the TGQD systems consist of the valence band (VB) states, the conduction band (CB) states, and the in-gap edge states. Before the pulse, all the VB states are initially populated and all the CB states are empty. For the edge states, below, we consider different cases with different numbers N_{PES} of populated edge states.

Interaction of an optical pulse with the electron system of the TGQD results in redistribution of electrons between the states of the TGQD. To characterize such a redistribution we introduce two characteristics that determine the electron populations of the excited states. The first one defines the number of excited electron in the conduction band states,

$$N_{EE,CB}(t) = \sum_{m\in CB} \tilde{\rho}_{mm}(t). \qquad (10)$$

Here the sum is over all TGQD CB states.

Another characteristics of the level of excitation is defined as the number of excited electrons in the CB states and in the initially empty edge states,

$$N_{EE}(t) = N_{EE,CB}(t) + \sum_{m\in ES, m\notin PES} \tilde{\rho}_{mm}(t), \qquad (11)$$

where ES means the edge states and PES means initially, i.e., before the pulse, populated edge states.

With the known solution of the density matrix equation (9) we can also find the time-dependent dipole moment from the following expression:

$$\mathbf{d}(t) = \sum_{mn} \tilde{\rho}_{mn}(t)e^{i\omega_{mn}t}\mathbf{D}_{nm}. \qquad (12)$$

The time variation of the dipole moment determines the radiation of the system. At a given frequency ω, the intensity of the corresponding radiation is given by the following expression,

$$I(\omega) = \frac{\mu_0\omega^2}{12\pi c}[|\mathcal{F}_\omega[\dot{d}_x]|^2 + |\mathcal{F}_\omega[\dot{d}_y]|^2], \qquad (13)$$

where $\mathcal{F}_\omega[\dot{d}_x]$ and $\mathcal{F}_\omega[\dot{d}_y]$ are frequency Fourier transforms of the time derivatives of the corresponding components of the dipole moment.

The order of the generated high harmonic is defined in units of ω_0, i.e.,

$$N_\omega = \frac{\omega}{\omega_0}. \qquad (14)$$

III. RESULTS AND DISCUSSION

We consider graphene QDs of triangular shape with zigzag edges. Such QDs are shown in Fig. 1 for two QD sizes, with 22 and 46 atoms in the dot. The energy spectra of TGQDs are obtained within the tight-binding model and are shown in Fig. 2. For all sizes of QDs, the edge states are clearly visible. They have zero energy and are degenerate. The number of edge states depends on the size of TGQD, where for 22-atom and 46-atom QDs the number of edge states is even, while for 33-atom QD this number is odd. Below, we will mainly study the QDs with even number of edge states.

In QDs, due to dimensional quantization, the energy spectra have a finite band gap, which separates the valence and conduction band states. Here we define the valence band states as the states with negative energies, while the conduction band states are the states with positive energies. For the sizes of the QDs that we consider below the band gap between the conduction and valence band states is around 4 eV. There are also degenerate in-gap edge states with zero energy. The edge states are mainly localized near the edges of QDs. The triangular graphene QDs have D_{3h} symmetry group, and the corresponding energy states are characterized by irreducible representation of D_{3h}, which are 1D A''_1 and A''_2 and 2D E''. All edge states belong to A''_2 representation, while the bulk conduction band and valence band states are mainly A''_1 and E''. There is a strong dipole coupling between the edge states and lowest CB and VB states, which belong to either A''_1 or E'' representations.

The edge states lower the effective band gap, making it close to 2 eV. Each level in Fig. 2 is double-degenerate due to spin. Below we are interested in the effects of edge state on the nonlinear optical properties of TGQDs. Thus, we consider the cases when all valence band states are fully occupied and
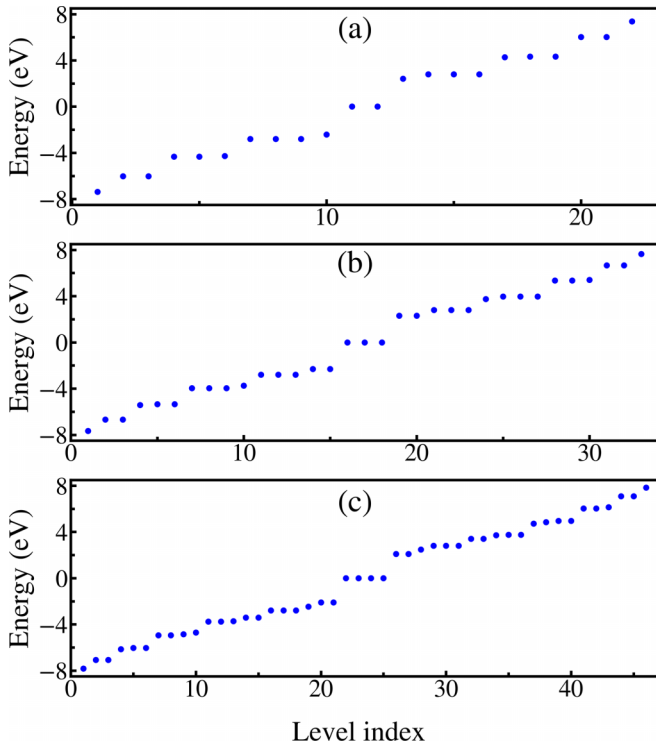
FIG. 2. Energy spectra of TGQDs consisting of 22 atoms (a), 33 atoms (b), and 46 atoms (c). States with positive energies belong to the conduction band, states with negative energies correspond to the valence band, and zero-energy degenerate states are the edge states. The number of edge states is two, three, and four for 22-, 33-, and 46-atom TGQDs, respectively.

FIG. 3. Panel (a): Profile of a linearly polarized optical pulse. The pulse amplitude is 0.1 V/Å and its frequency is $\hbar\omega_0 = 1$ eV. The pulse is polarized in the x direction. The corresponding generated dipole moment is shown in panels (b) (x component) and (c) (y component) as a function of time. The number of atoms in the quantum dot is 46. No edge states are populated before the pulse.

the in-gap edge states are partially occupied. Therefore, all valence band states, i.e., both spin-up and spin-down states, are occupied, and the population of the edge states follows the Hund's rule, which means that extra electrons first populate the degenerate edge states with one spin component, for example a spin-up component. Thus, below we consider the following situation: for a spin-down component, all valence band states are populated and edge states are empty, while for a spin-up component, all valence band states and N_{PES} edge states are populated. We change the population of the edge states to see their effect on the nonlinear optical response of graphene QDs. Since the populations of the spin-down electron states remain the same, below we study only the response due to spin-up states with variable population of the edge states.

For triangular graphene QDs shown in Fig. 1, only the y axis is the axis of symmetry. In this case, if a linearly polarized incident optical pulse is y polarized then the generated dipole moment has only the y component, while if an incident pulse is x polarized, then both x and y components of the generated dipole moment are nonzero. First we analyze the response of the system to the pulse polarized in the x direction. The profile of the corresponding electric field and the x and y components of the generated dipole moment are shown in Fig. 3. While the x component of the dipole moment follows the profile of the electric field of the pulse, the y component of the dipole moment shows high frequency oscillations.
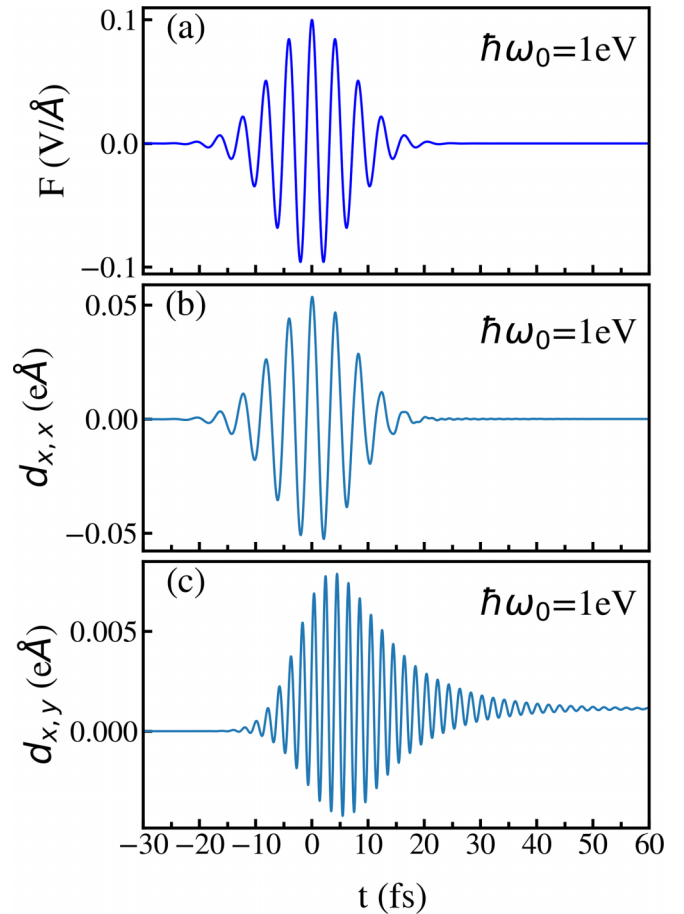
The strongest interlevel coupling and the corresponding interlevel electron transfer is realized between the states with the smallest energy separation, i.e., between the valence band states and the edge states and between the edge states and the conduction band states. Such couplings determine the leading contribution to the nonlinear electron dynamics in the field of the pulse. To illustrate this property we show in Fig. 4 the time-dependent populations $N_{EE}(t)$ and $N_{EE,CB}(t)$ for different values of N_{PES}. The results are shown for a 22-atom QD with two edge states but similar results are expected for other sizes of TGQD. When the edge states are not initially populated, see Fig. 4(a), then the main electron transfer occurs between the valence band states and the edge states; i.e., the total population of the conduction band states is small, around 0.01, while the population of the edge states is relatively large, around 0.1. Here the number 0.1 describes the electron transfer to the two edge states, which means that the electron transfer to one edge state is 0.05. If only one edge state is populated, see Fig. 4(b), then the total number of electrons transferred to the conduction band is 0.05, which is similar to the number of electrons transferred from the valence band states to the edge states in case (a). If both edge states are occupied,
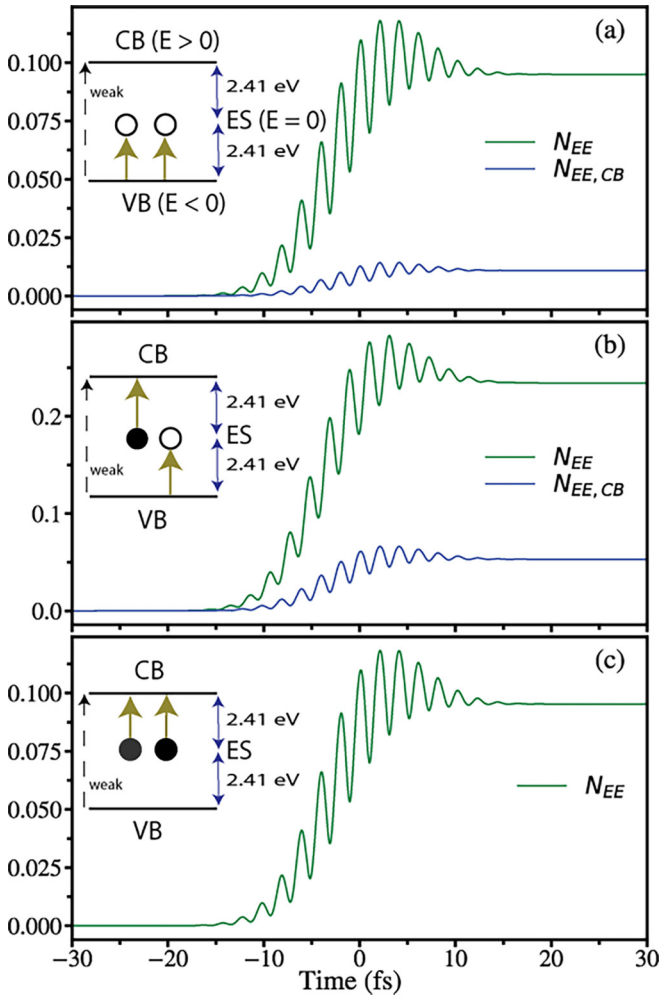
FIG. 4. Populations of the excited states, N_{EE} and $N_{EE,CB}$, as a function of time. Panel (a): No edge states are initially populated. Panel (b): One edge state is populated before the pulse. Panel (c): All edge states are populated before the pulse. The filled dots in the inset represent the populated edge states and the open dots describe the empty edge states. The frequency of the pulse is $\hbar\omega_0 = 1$ eV and the pulse amplitude is 0.3 V/Å. The number of atoms in the quantum dot is 22.
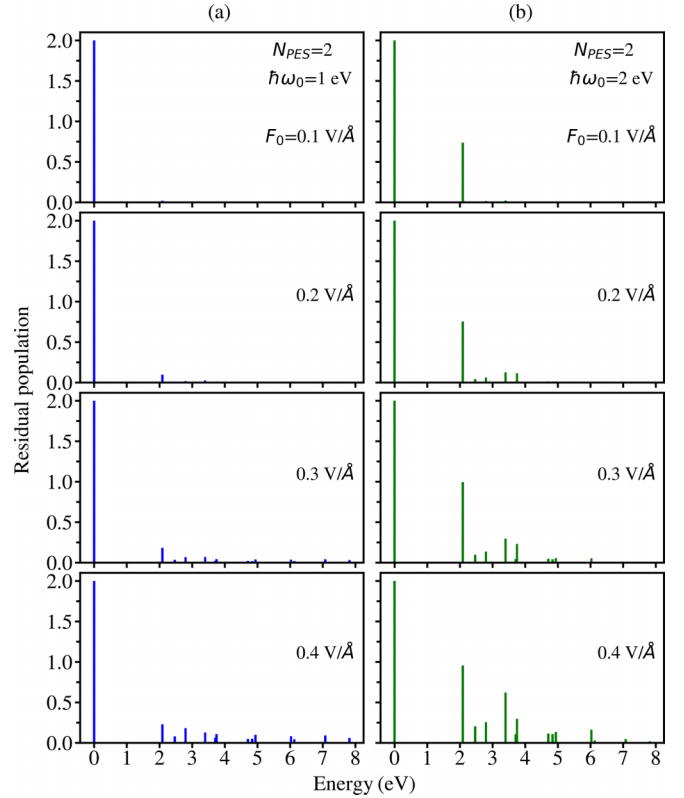

FIG. 5. Residual populations of the conduction band states and the edge states. Two edge states are populated before the pulse. The number of atoms in TGQD is 46. The corresponding pulse amplitude is marked in each panel. The frequency of the pulse is $\hbar\omega_0 = 1$ eV (a) and $\hbar\omega_0 = 2$ eV (b).

see Fig. 4(c), then the number of electrons transferred from the edge states to the conduction band states is around 0.1, which is similar to the total number of electrons transferred from the valence band states to the edge states in case (a).

The strength of the interlevel electron transfer depends on the frequency of the pulse. In Fig. 5, the residual populations of the conduction band states and the edge states are shown for two different frequencies of the pulse and its different amplitudes. The QD consists of 22 atoms and has two edge states. Initially, all edge states are populated. For all parameters of the pulse, the residual populations of the edge states remain the same, which means that the electron transfer from the edge states to the conduction band states is compensated by the electron transfer from the valence band states to the edge states. Also, for larger frequency of the pulse, $\hbar\omega_0 = 2$ eV, which is almost in the resonance with the edge states to the conduction band states transitions, the residual populations of

the conduction band states are relatively large. As expected, mainly the lower-energy conduction band states are populated.

The emission spectra of TGQDs for a linearly polarized pulse in the x direction are shown in Fig. 6 for different sizes of TGQDs and different initial populations of the edge states. Due to particle-hole symmetry of the system, the results when N_{PES} and $N_{edge} - N_{PES}$ edge states are populated are the same. Here N_{edge} is the total number of edge states. For example, for a 46-atom QD with four edge states, the emission spectra for the systems with 1 edge state populated and 3 edge states populated are identical. Therefore, in Fig. 6 and in all other figures below, only the data for $N_{PES} \leqslant N_{edge}/2$ are shown. The general tendency that can be seen in Fig. 6 is suppression of generation of even harmonics when the edge states are populated, i.e., when $N_{PES} > 0$. Such suppression is very strong when half of the edge states are initially populated. This is the case for 22-atom QDs with two edge states, see Fig. 6(a), where for $N_{PES} = 1$, there is a strong suppression of even harmonics compared to the $N_{PES} = 0$ case. Also, for 46-atom QDs with four edge states, strong suppression of even harmonics is realized for $N_{PES} = 2$; see Fig. 6(c). Population of half of the edge states is possible only for the systems with even number of edge states, e.g., for 22-atom and 46-atom QDs, but not for 33-atom QDs with three edge states.

In Fig. 7, the HHG spectra are shown for the systems with even number of edge states and for different amplitudes of the
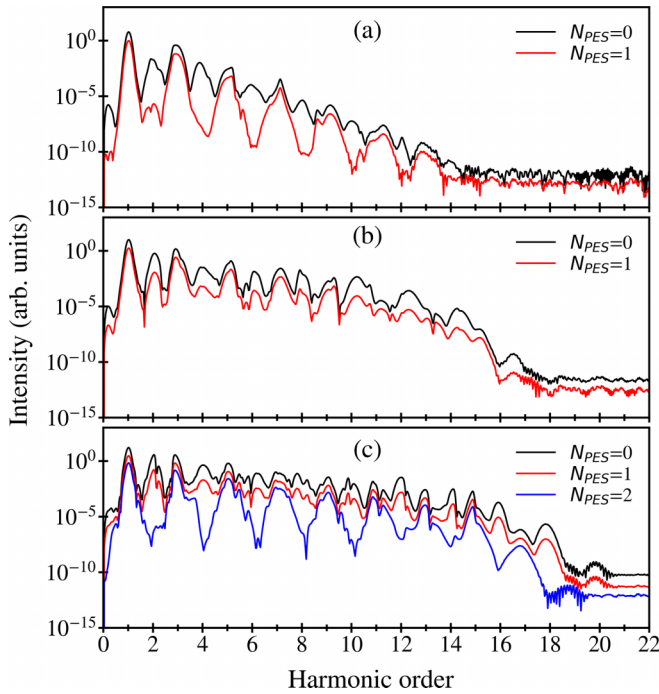
FIG. 6. Emission spectra of TGQDs. The number of atoms in the dot is 22 (a), 33 (b), and 46 (c). High harmonics with well-defined cutoffs are clearly visible in each spectrum. The numbers of populated edge states are marked for each graph. The frequency of the pulse is $\hbar\omega_0 = 1$ eV. The dephasing time is $\tau = 10$ fs. An offset was introduced to make the plotted data more readable.
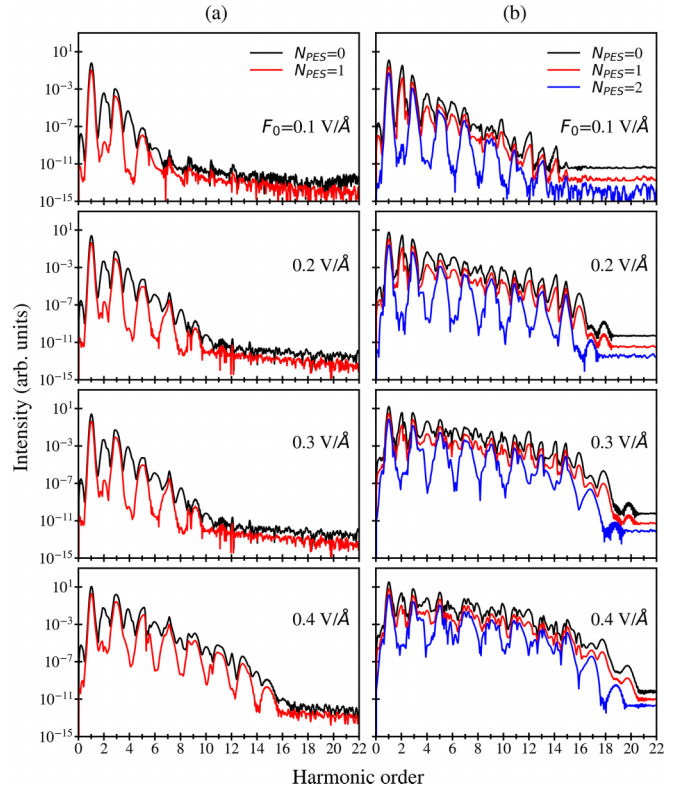

FIG. 7. Emission spectrum of TGQDs: The number of atoms is 22 (a) and 46 (b). High harmonics with well-defined cutoffs are clearly visible in the spectra. The corresponding populated edge states are marked for each graph. The frequency of the pulse is $\hbar\omega_0 = 1$ eV. With the increasing size of TGQDs, the number of harmonics as well as the cutoff frequency increase. The dephasing time is $\tau = 10$ fs. An offset was introduced to make the plotted data more readable.

optical pulse with the frequency of the pulse $\hbar\omega_0 = 1$ eV. For all cases, the even harmonics are strongly suppressed when the edge states are initially half filled. The suppression is more pronounced for smaller field amplitudes when mainly the low-energy conduction band states are populated during the pulse and strongly contribute to generation of high harmonics. Thus, the suppression of high harmonics is mainly determined by the lower-energy conduction band states. Since the population of the conduction band states during the pulse is sensitive to the frequency of the pulse, i.e., at higher frequencies, which are closer to the band gap, more conduction band states are populated during the pulse, the suppression of high harmonics should be sensitive to the frequency of the incident pulse.

In Fig. 8, the radiation spectra are shown for incident pulses with the frequencies that are comparable to the interlevel energy separation between the edge states and the conduction band states. In this case, the suppression of even harmonics at half filling of the edge states is not that strong compared to the low-frequency pulses and the peaks corresponding to even harmonics are clearly visible. For such frequencies of the pulse, there is a relatively strong population of high-energy conduction band levels during the pulse. Also, similarly to a low-frequency pulse, suppression of even harmonics becomes less pronounced for high field amplitude. Thus, the suppression of even harmonics, when half of the edge states are populated, is less pronounced when high-energy conduction band levels are excited during the pulse, which happens when the frequency of the pulse is close to the resonant condition or when the amplitude of the pulse is large.

The total radiation spectra produced by TGQDs have two contributions, which come from the x and y components of the dipole moment. Since for a TGQD only the y axis is the axis of symmetry, the pulse polarized in the x direction generates the dipole moment, which has both the x and y components. The corresponding contributions, $I_{x,x}$ and $I_{x,y}$, to the radiation spectra are shown in Fig. 9 for a 46-atom QD and different initial populations of the edge states. Here $I_{x,x}$ is determined by the x component of the dipole moment, while $I_{x,y}$ is due to the y component of the dipole moment. Since the y axis is the axis of symmetry of the system, then $I_{x,x}$ has only odd harmonics, see black lines in Fig. 9, and $I_{x,y}$ shows only even harmonics, see red lines in Fig. 9. In general, both contributions, $I_{x,x}$ and $I_{x,y}$, have comparable magnitudes, see Figs. 9(a) and 9(b) where $N_{PES} = 0$ and $N_{PES} = 1$, which results in comparable intensities of both even and odd harmonics in the total radiation spectra. When half of the edge states are populated, see Fig. 9(c), then $I_{x,y}$ becomes strongly suppressed, which results in suppression of the intensities of even harmonics in the total radiation spectrum.

All the above results correspond to optical pulses polarized along the x direction. For a pulse polarized along the y direction, which is the axis of symmetry of the system, only the y component of the dipole moment is generated during
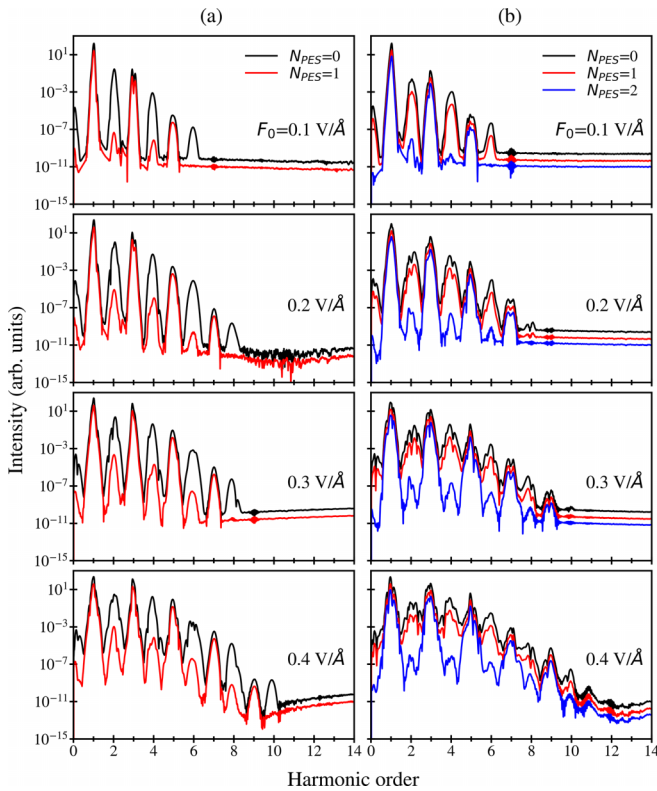
FIG. 8. Emission spectra of TGQDs. Column (a) corresponds to 22-atom TGQD, while column (b) describes the 46-atom TGQD. The number of populated edge states are marked for each graph. The amplitudes of the optical pulses are also shown in each panel. The frequency of the pulse is $\hbar\omega_0 = 2.3$ eV in column (a) and $\hbar\omega_0 = 2$ eV in column (b). With increasing the size of TGQDs, the number of generated harmonics increases. The dephasing time is $\tau = 10$ fs. An offset was introduced to make the plotted data more readable.
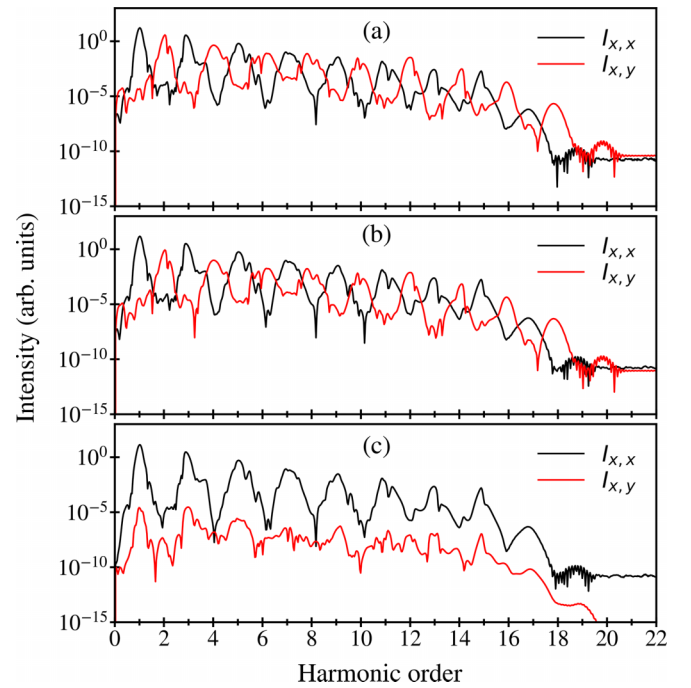

FIG. 9. Radiation spectra due to x and y components of the dipole moment. The incident pulse is linearly polarized in the x direction. The radiation spectra labeled by $I_{x,x}$ are determined by the x component of the dipole moment, while the radiation spectra $I_{x,y}$ are due to the y component of the dipole moment. The number of atoms in TGQD is 46. Panel (a): No edge states are populated; panel (b): one edge state is populated; and panel (c): two edge states are populated before the pulse. The radiation spectra $I_{x,x}$ have only odd components, while radiation spectra $I_{x,y}$ have only even components. The contributions to the radiation spectra associated with the y component of the dipole moment are suppressed significantly when two edge states are initially populated. The dephasing time is $\tau = 10$ fs. The frequency of the pulse is $\hbar\omega_0 = 1$ eV and its amplitude is $F_0 = 0.3$ V/Å.

the pulse, while the x component is zero. In general, for a pulse polarized in the y direction, all high harmonic orders are generated. At the same time, similar to the case of a pulse polarized in the x direction, when the edge states are half filled, the even harmonics are strongly suppressed. In Fig. 10 we present comparison of the results for two polarizations of the incident pulse: x and y. For all cases, for the low harmonics, the radiation spectra are very similar with comparable intensities. For high harmonics, the x-polarized pulse produces much more intense harmonics than the y-polarized pulse does. Also, the cutoff frequency is larger for the x-polarized pulse. Thus, the main difference between the x and y polarized pulses is visible at harmonics with large frequencies, $> 10\omega_0$. The results in Fig. 10 are shown for the pulse frequency of $\hbar\omega_0 = 1$ eV when harmonics of up to 20th order can be generated. For larger frequency of the pulse, e.g., $\hbar\omega_0 = 2$ eV, the condition is close to the resonant one and a low number of harmonics is generated. In this case the radiation spectra are almost the same for both x and y polarized pulses.

Suppression of even-order harmonics reported above occurs when the edges states of graphene QDs are half filled. Such a system also has a particle-hole symmetry. The edge states, which belong to the A_2'' representation of the D_{3h} symmetry group, are strongly coupled by a linearly polarized

optical pulse to the lowest CB and the highest VB states, which belong to the A_1'' and E'' representations. At the same time, the direct dipole coupling between the CB and VB states with the same symmetry is suppressed. In this case, in the field of the pulse, the electron transfer from the VB to the CB states occurs through the edge states. Because of the particle-hole symmetry of the system, the amount of the electron transfer from the VB states to the edge states is the same as the corresponding transfer from the edge states to the CB states. Thus, during the pulse, the edge states stay half filled and effectively electrons are transferred between the highest-energy VB states and the lowest-energy CB states with the same symmetry. As a result, the y component of the dipole moment, which is responsible for the even-order harmonics, is suppressed. Such suppression becomes less pronounced for the pulses with high frequency, when the coupling between the CB and the VB states occurs not only through the edge states but also directly between the states of different symmetries, i.e., A_1'' and E''.

One of the important characteristics of the HHG is the harmonic cutoff, which is the maximum harmonic order that can be generated. The cutoff frequency as a function of the field amplitude, F_0, is shown in Fig. 11 for different systems
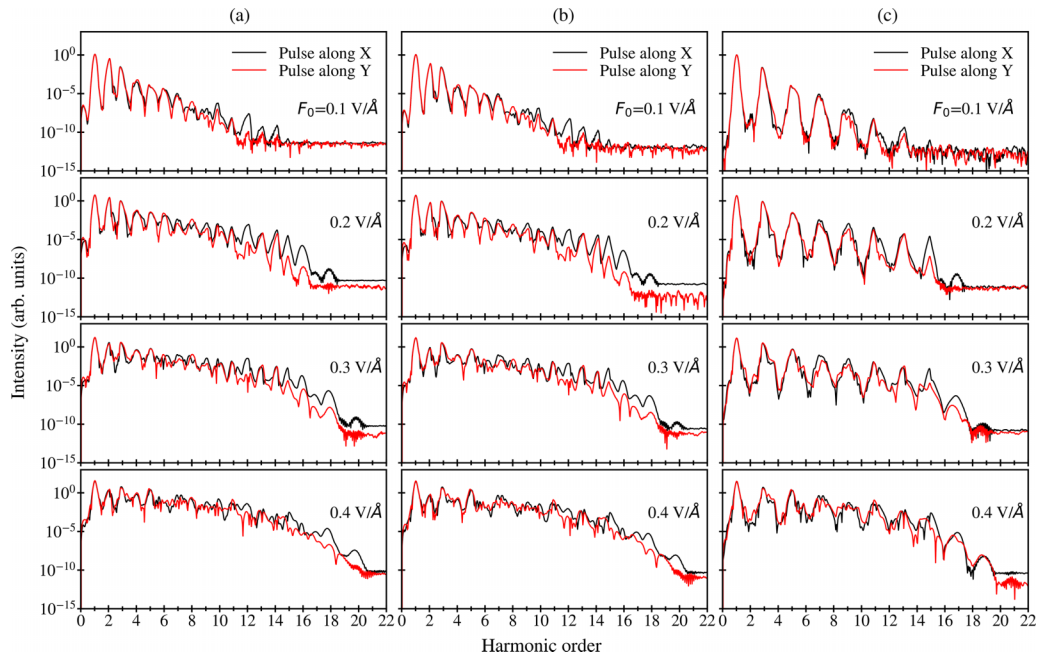
FIG. 10. Radiation spectra of TGQD consisting of 46 atoms in the field of a linearly polarized pulse. The spectra corresponding to the pulses polarized along the x and y directions are shown by the red and black lines, respectively. The amplitudes of the corresponding optical pulses are shown in each panel. Different columns have different numbers of populated edge states before the pulse. Column (a): No edge states are populated; column (b): one edge state is populated; and column (c): two edge states are populated. The frequency of the pulse is $\hbar\omega_0 = 1$ eV. The dephasing time is $\tau = 10$ fs.

and different numbers of populated edge states. For almost all cases, the cutoff frequency has linear dependence on F_0. Such linear dependence is more clearly pronounced for high frequency of the incident pulse. Another property is that, generally, with increasing the initial population of the edge states the cutoff frequency decreases. This is due to decrease of the number of available states for electron excitations when the number of edge states increases. Also, with increasing size of the system, from 22 to 46, the cutoff frequency monotonically increases, which is related to the corresponding increase in the number of electron states, both occupied and empty, in the QD system with increasing QD size.
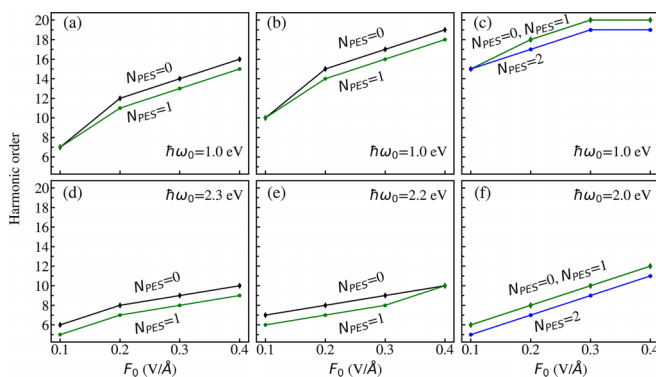

FIG. 11. Harmonic cutoff versus the amplitude of the optical pulse. The frequency of the pulse is $\hbar\omega_0 = 1$ eV (a), (b), and (c); 2.3 eV (d); 2.2 eV (e); and 2 eV (f). The numbers of populated edge states are shown next to the corresponding lines in each panel.

IV. CONCLUSION

The radiation spectra of TGQDs placed in the field of an optical pulse depend on the size of the system and also on the parameters of the optical pulse, its amplitude, and frequency. Another characteristic of graphene QDs that can control the radiation spectrum and the corresponding generation of high harmonics is an initial electron population of QD edge states. Such edge states exist in graphene QDs with zigzag edges. Since the edge states in such systems are in-gap states, they can strongly affect the generation of high harmonics. Namely, the generation of high harmonics depends on the number of initially occupied edge states. The strongest effect is observed for the systems, i.e., TGQDs with zigzag edges, which have an even number of edge states. In this case, if half of the edge states with the same spin component are initially populated then even high harmonics in the radiation spectra are suppressed. The level of suppression strongly depends on the frequency of the pulse. If the frequency of the pulse is close to the resonant condition, i.e., to the energy difference between the edge states and the conduction band states, then the even harmonics are weakly suppressed and the corresponding peaks in the emission spectra are clearly visible. But if the frequency of the pulse is small and far from the resonant condition, then suppression of even harmonics is strong with almost no peaks visible in radiation spectra at even frequencies.

The suppression of even harmonics at half-filled edge states is almost the same for different polarizations of the incident pulse, i.e., for x and y linearly polarized pulses.

Strong suppression of even harmonics in radiation spectra of TGQDs at a specific filling of TGQD edge states opens the

possibility of control of the intensity of high harmonics by variation of gate voltage.

[1] J. L. Krause, K. J. Schafer, and K. C. Kulander, High-Order Harmonic Generation from Atoms and Ions in the High Intensity Regime, Phys. Rev. Lett. **68**, 3535 (1992).

[2] D. von der Linde, T. Engers, G. Jenke, P. Agostini, G. Grillon, E. Nibbering, A. Mysyrowicz, and A. Antonetti, Generation of high-order harmonics from solid surfaces by intense femtosecond laser pulses, Phys. Rev. A **52**, R25 (1995).

[3] P. A. Norreys, M. Zepf, S. Moustaizis, A. P. Fews, J. Zhang, P. Lee, M. Bakarezos, C. N. Danson, A. Dyson, P. Gibbon, P. Loukakos, D. Neely, F. N. Walsh, J. S. Wark, and A. E. Dangor, Efficient Extreme UV Harmonics Generated from Picosecond Laser Pulse Interactions with Solid Targets, Phys. Rev. Lett. **76**, 1832 (1996).

[4] S. Ghimire, A. D. DiChiara, E. Sistrunk, P. Agostini, L. F. DiMauro, and D. A. Reis, Observation of high-order harmonic generation in a bulk crystal, Nat. Phys. **7**, 138 (2011).

[5] G. Vampa, T. J. Hammond, N. Thiré, B. E. Schmidt, F. Légaré, C. R. McDonald, T. Brabec, and P. B. Corkum, Linking high harmonics from gases and solids, Nature (London) **522**, 462 (2015).

[6] G. Ndabashimiye, S. Ghimire, M. Wu, D. A. Browne, K. J. Schafer, M. B. Gaarde, and D. A. Reis, Solid-state harmonics beyond the atomic limit, Nature (London) **534**, 520 (2016).

[7] H. Liu, Y. Li, Y. S. Yu, S. Ghimire, T. F. Heinz, and D. A. Reis, High-harmonic generation from an atomically thin semiconductor, Nat. Phys. **13**, 262 (2017).

[8] Y. S. You, Y. Yin, Y. Wu, A. Chew, X. Ren, F. Zhuang, S. Gholam-Mirzaei, M. Chini, Z. Chang, and S. Ghimire, High-harmonic generation in amorphous solids, Nat. Commun. **8**, 724 (2017).

[9] N. Klemke, N. Tancogne-Dejean, G. M. Rossi, Y. Yang, F. Scheiba, R. E. Mainz, G. Di Sciacca, A. Rubio, F. X. Kärtner, and O. D. Mücke, Polarization-state-resolved high-harmonic spectroscopy of solids, Nat. Commun. **10**, 1319 (2019).

[10] M. Lewenstein, Ph. Balcou, M. Y. Ivanov, A. L'Huillier, and P. B. Corkum, Theory of high-harmonic generation by low-frequency laser fields, Phys. Rev. A **49**, 2117 (1994).

[11] D. Golde, T. Meier, and S. W. Koch, High harmonics generated in semiconductor nanostructures by the coupled dynamics of optical inter- and intraband excitations, Phys. Rev. B **77**, 075330 (2008).

[12] N. Klemke, O. D. Mücke, A. Rubio, F. X. Kärtner, and N. Tancogne-Dejean, Role of intraband dynamics in the generation of circularly polarized high harmonics from solids, Phys. Rev. B **102**, 104308 (2020).

[13] I. Kilen, M. Kolesik, J. Hader, J. V. Moloney, U. Huttner, M. K. Hagen, and S. W. Koch, Propagation Induced Dephasing in Semiconductor High-Harmonic Generation, Phys. Rev. Lett. **125**, 083901 (2020).

[14] F. Krausz and M. Ivanov, Attosecond physics, Rev. Mod. Phys. **81**, 163 (2009).

[15] S. Y. Kruchinin, F. Krausz, and V. S. Yakovlev, *Colloquium:* Strong-field phenomena in periodic systems, Rev. Mod. Phys. **90**, 021002 (2018).

[16] A. Schiffrin, T. Paasch-Colberg, N. Karpowicz, V. Apalkov, D. Gerster, S. Muhlbrandt, M. Korbman, J. Reichert, M. Schultze, S. Holzner, J. V. Barth, R. Kienberger, R. Ernstorfer, V. S. Yakovlev, M. I. Stockman, and F. Krausz, Optical-field-induced current in dielectrics, Nature (London) **493**, 70 (2013).

[17] J. Kiemle, P. Zimmermann, A. W. Holleitner, and C. Kastl, Light-field and spin-orbit-driven currents in van der Waals materials, Nanophotonics **9**, 2693 (2020).

[18] T. Paasch-Colberg, A. Schiffrin, N. Karpowicz, S. Kruchinin, S. Ozge, S. Keiber, O. Razskazovskaya, S. Muhlbrandt, A. Alnaser, M. Kubel, V. Apalkov, D. Gerster, J. Reichert, T. Wittmann, J. V. Barth, M. I. Stockman, R. Ernstorfer, V. S. Yakovlev, R. Kienberger, and F. Krausz, Solid-state light-phase detector, Nat. Photonics **8**, 214 (2014).

[19] T. Higuchi, C. Heide, K. Ullmann, H. B. Weber, and P. Hommelhoff, Light-field-driven currents in graphene, Nature (London) **550**, 224 (2017).

[20] E. Gruber, R. A. Wilhelm, R. Pétuya, V. Smejkal, R. Kozubek, A. Hierzenberger, B. C. Bayer, I. Aldazabal, A. K. Kazansky, F. Libisch, A. V. Krasheninnikov, M. Schleberger, S. Facsko, A. G. Borisov, A. Arnau, and F. Aumayr, Ultrafast electronic response of graphene to a strong and localized electric field, Nat. Commun. **7**, 13948 (2016).

[21] S. Sederberg, D. Zimin, S. Keiber, F. Siegrist, M. S. Wismer, V. S. Yakovlev, I. Floss, C. Lemell, J. Burgdörfer, M. Schultze, F. Krausz, and N. Karpowicz, Attosecond optoelectronic field measurement in solids, Nat. Commun. **11**, 430 (2020).

[22] G. Vampa, J. Lu, Y. S. You, D. R. Baykusheva, M. Wu, H. Liu, K. J. Schafer, M. B. Gaarde, D. A. Reis, and S. Ghimire, Attosecond synchronization of extreme ultraviolet high harmonics from crystals, J. Phys. B: At. Mol. Opt. Phys. **53**, 144003 (2020).

[23] M. Trushin, A. Grupp, G. Soavi, A. Budweg, D. De Fazio, U. Sassi, A. Lombardo, A. C. Ferrari, W. Belzig, A. Leitenstorfer, and D. Brida, Ultrafast pseudospin dynamics in graphene, Phys. Rev. B **92**, 165429 (2015).

[24] S. A. Oliaei Motlagh, J.-S. Wu, V. Apalkov, and M. I. Stockman, Femtosecond valley polarization and topological resonances in transition metal dichalcogenides, Phys. Rev. B **98**, 081406(R) (2018).

[25] D. Sun, J. W. Lai, J. C. Ma, Q. S. Wang, and J. Liu, Review of ultrafast spectroscopy studies of valley carrier dynamics in two-dimensional semiconducting transition metal dichalcogenides, Chin. Phys. B **26**, 037801 (2017).

[26] F. Gesuele, Ultrafast hyperspectral transient absorption spectroscopy: Application to single layer graphene, Photonics **6**, 95 (2019).

[27] J. Zhang, H. Ouyang, X. Zheng, J. You, R. Chen, T. Zhou, Y. Sui, Y. Liu, X. Cheng, and T. Jiang, Ultrafast saturable absorption of MoS_2 nanosheets under different pulse-width excitation conditions, Opt. Lett. **43**, 243 (2018).

[28] R. C. Ashoori, Electrons in artificial atoms, Nature (London) **379**, 413 (1996).

[29] T. Chakraborty, *Quantum Dots* (Elsevier, Amsterdam, 1999).

[30] Y. Arakawa and H. Sakaki, Multidimensional quantum well laser and temperature dependence of its threshold current, Appl. Phys. Lett. **40**, 939 (1982).

[31] D. Loss and D. P. DiVincenzo, Quantum computation with quantum dots, Phys. Rev. A **57**, 120 (1998).

[32] X. Michalet, F. F. Pinaud, L. A. Bentolila, J. M. Tsay, S. Doose, J. J. Li, G. Sundaresan, A. M. Wu, S. S. Gambhir, and S. Weiss, Quantum dots for live cells, in vivo imaging, and diagnostics, Science **307**, 538 (2005).

[33] V. Veeramani, Z. Bao, M.-H. Chan, H.-C. Wang, A. Jena, H. Chang, S.-F. Hu, and R.-S. Liu, Quantum dots for light conversion, therapeutic and energy storage applications, J. Solid State Chem. **270**, 71 (2019).

[34] Q. Liu, J. Sun, K. Gao, N. Chen, X. Sun, D. Ti, C. Bai, R. Cui, and L. Qu, Graphene quantum dots for energy storage and conversion: From fabrication to applications, Mater. Chem. Front. **4**, 421 (2020).

[35] K. K. Hansen, D. Bauer, and L. B. Madsen, Finite-system effects on high-order harmonic generation: From atoms to solids, Phys. Rev. A **97**, 043424 (2018).

[36] D. Pan, J. Zhang, Z. Li, and M. Wu, Hydrothermal route for cutting graphene sheets into blue-luminescent graphene quantum dots, Adv. Mater. **22**, 734 (2010).

[37] S. Chung, R. A. Revia, and M. Zhang, Graphene quantum dots and their applications in bioimaging, biosensing, and therapy, Adv. Mater. **33**, 1904362 (2021).

[38] H. Sun, L. Wu, W. Wei, and X. Qu, Recent advances in graphene quantum dots for sensing, Mater. Today **16**, 433 (2013).

[39] M. Bacon, S. J. Bradley, and T. Nann, Graphene quantum dots, Part. Part. Syst. Charact. **31**, 415 (2014).

[40] K. S. Novoselov, A. K. Geim, S. V. Morozov, D. Jiang, Y. Zhang, S. V. Dubonos, I. V. Grigorieva, and A. A. Firsov, Electric field effect in atomically thin carbon films, Science **306**, 666 (2004).

[41] A. K. Geim and K. S. Novoselov, The rise of graphene, Nat. Mater. **6**, 183 (2007).

[42] A. H. Castro Neto, F. Guinea, N. M. R. Peres, K. S. Novoselov, and A. K. Geim, The electronic properties of graphene, Rev. Mod. Phys. **81**, 109 (2009).

[43] D. S. L. Abergel, V. Apalkov, J. Berashevich, K. Ziegler, and T. Chakraborty, Properties of graphene: A theoretical perspective, Adv. Phys. **59**, 261 (2010).

[44] S. Das Sarma, S. Adam, E. H. Hwang, and E. Rossi, Electronic transport in two-dimensional graphene, Rev. Mod. Phys. **83**, 407 (2011).

[45] A. F. Young and P. Kim, Electronic transport in graphene heterostructures, Annu. Rev. Condens. Matter Phys. **2**, 101 (2011).

[46] H. K. Kelardeh, V. Apalkov, and M. I. Stockman, Graphene in ultrafast and superstrong laser fields, Phys. Rev. B **91**, 045439 (2015).

[47] S. A. Oliaei Motlagh, F. Nematollahi, V. Apalkov, and M. I. Stockman, Topological resonance and single-optical-cycle valley polarization in gapped graphene, Phys. Rev. B **100**, 115431 (2019).

[48] S. A. Oliaei Motlagh and V. Apalkov, Absorption properties of graphene quantum dots under ultrashort optical pulses, Phys. Rev. B **104**, 045421 (2021).

[49] S. Gnawali, R. Ghimire, K. R. Magar, S. J. Hossaini, and V. Apalkov, Ultrafast electron dynamics of graphene quantum dots: High harmonic generation, Phys. Rev. B **106**, 075149 (2022).

[50] J. Fernández-Rossier and J. J. Palacios, Magnetism in graphene nanoislands, Phys. Rev. Lett. **99**, 177204 (2007).

[51] K. Nakagawa, H. Hirori, S. A. Sato, H. Tahara, F. Sekiguchi, G. Yumoto, M. Saruyama, R. Sato, T. Teranishi, and Y. Kanemitsu, Size-controlled quantum dots reveal the impact of intraband transitions on high-order harmonic generation in solids, Nat. Phys. **18**, 874 (2022).